International Journal of Nanomedicine

Dovepress
open access to scientific and medical research

Open Access Full Text Article

ORIGINAL RESEARCH

# Combined Hydroxyethyl Starch Luteolin Nanocrystals for Effective Anti-Hyperuricemia Effect in Mice Model

Han Luo[1,*], Xiaofei Wang[1,*], Mengqi Fang[1], Huifan Yu[1], Lili Gui[1], Zhengkun Wu[1], Jianyong Sheng[2], Fei Li[1]

[1]Hubei Key Laboratory of Wudang Local Chinese Medicine Research, School of Pharmaceutical Sciences, Hubei University of Medicine, Shiyan, Hubei, People's Republic of China; [2]Key Laboratory of Smart Drug Delivery, Ministry of Education, Department of Pharmaceutics, School of Pharmacy, Fudan University, Shanghai, People's Republic of China

*These authors contributed equally to this work

Correspondence: Fei Li, Hubei University of Medicine, 30 Renmin South Road, Shiyan, Hubei, 442000, People's Republic of China, Email piaopodexinlifei@163.com

International Journal of Nanomedicine downloaded from https://www.dovepress.com/
For personal use only.

**Introduction:** Although flavonoid compounds exhibit various pharmacological activities, their clinical applications are restricted by low oral bioavailability owing to their poor solubility. Nanocrystals (NCs) represent an excellent strategy for enhancing the oral bioavailability of flavonoids. Hydroxyethyl starch (HES), a biomaterial compound used as a plasma expander, could be an ideal stabilizer material for preparing flavonoid NCs.

**Methods:** HES was used to stabilize flavonoid nanocrystals (NCs), using luteolin (LUT) as a model drug. After full characterization, the freeze-drying and storage stability, solubility, intestinal absorption, pharmacokinetics, and in vivo anti-hyperuricemic effect of the optimized HES-stabilized LUT NCs (LUT-HES NCs) were investigated.

**Results:** Uniformed LUT-HES NCs were prepared with mean particle size of 191.1±16.8 nm, zeta potential of about −23 mV, drug encapsulation efficiency of 98.52 ± 1.01%, and drug loading of 49.26 ± 0.50%. The freeze-dried LUT-HES NCs powder showed good re-dispersibility and storage stability for 9 months. Notably, compared with the coarse drug, LUT-HES NCs exhibited improved saturation solubility (7.49 times), increased drug dissolution rate, enhanced Caco-2 cellular uptake (2.78 times) and oral bioavailability (Fr=355.7%). Pharmacodynamic studies showed that LUT-HES NCs remarkably lowered serum uric acid levels by 69.93% and ameliorated renal damage in hyperuricemic mice.

**Conclusion:** HES is a potential stabilizer for poorly soluble flavonoid NCs and provides a promising strategy for the clinical application of these compounds. LUT-HES NCs may be an alternative or complementary strategy for hyperuricemia treatment.

**Keywords:** Hydroxyethyl starch, nanocrystals, stabilizer, luteolin, oral bioavailability, anti-hyperuricemia

## Introduction

Flavonoids represent a class of secondary metabolites with polyphenol structure, such as luteolin, quercetin, rutin, hesperidin and phloretin, which are widely found in fruits, vegetables, tea and Chinese herbal medicine.[1,2] Flavonoids are generally characterized by the C6-C3-C6 basic skeleton, composed of two benzene rings with phenolic hydroxyl connected by a central chain of three-carbon atoms.[3,4] Due to the unique chemical structure, flavonoids possess a variety of activities including antioxidant, anti-inflammatory, anti-tumor, hypoglycemic, uric acid-lowering, antibacterial and antiviral properties, which play a vital role in maintaining human and animal health.[1,5–8] These natural compounds are a group of promising drug candidates that warrant further exploration. Unfortunately, the application of flavonoids in disease prevention and/or treatment is unsatisfactory, probably because of their poor aqueous solubility and limited oral bioavailability.[3,9–11]

Nanocrystals (NCs), also called nanosuspensions, is a submicron colloidal dispersion system composed of "pure drugs" with stabilizer, which has been considered a brilliant strategy to enhance the oral bioavailability of insoluble

Received: 20 February 2024
Accepted: 21 May 2024
Published: 4 June 2024



© 2024 Luo et al. This work is published and licensed by Dove Medical Press Limited. The full terms of this license are available at https://www.dovepress.com/terms.php and incorporate the Creative Commons Attribution – Non Commercial (unported, v3.0) License (http://creativecommons.org/licenses/by-nc/3.0/). By accessing the work you hereby accept the Terms. Non-commercial uses of the work are permitted without any further permission from Dove Medical Press Limited, provided the work is properly attributed. For permission for commercial use of this work, please see paragraphs 4.2 and 5 of our Terms (https://www.dovepress.com/terms.php).

active flavonoid components.[10,12,13] By directly reducing the particle size of these compounds to the nanometer range and thus enlarging their surface area, this strategy can increase the saturation solubility and dissolution velocity, eventually realizing improved bioavailability and expanding scope of application.[14–16] Stabilizer is generally required to prevent aggregation between high-energy crystal surfaces during size reduction during nanocrystals preparation.[17,18] However, there is no systematic screening rule for the types, dosage and prescription of stabilizers for flavonoid NCs, so the screening of stabilizers is mainly based on the exclusion method at present.[12,19] On the other hand, the commonly used stabilizers for nanosuspensions including sodium dodecyl sulfate and Tween 80 have the drawbacks of poor biocompatibility and chronic toxicity.[10,18,20] In addition, nanosuspensions are usually transformed into solid nanocrystals to increase their storage stability and considerable amounts of extra cryoprotectants is introduced to prevent the irreversible agglomeration of particles during the freeze-drying solidification process,[21] leading to low drug content of the final product and increased chemical burden to the patient and exacerbated potential toxicity.[10]

Hydroxyethyl starch (HES) is a semisynthetic polysaccharide derived from the hydrolysis of waxy corn followed by hydroxyethylation.[22] It has been used as a biomedical material with a long history, such as plasma expender and cell cryopreservation, owing to its fast and powerful volume expansion effect and ability to absorb water molecules without phase transition during cooling.[22–25] Of note, HES can be degraded in vivo because the α-1,4 glycosidic linkages of HES connecting the sugar unit can be cut off by α-amylase in the blood.[26] In particular, hydrogen bonds can be formed between the hydroxyl functional groups in HES and the phenolic hydroxyl groups in flavonoids.[19] Therefore, HES could be an ideal stabilizer and cryoprotectant to prepare and solidify flavonoid NCs because of its unique structure and characteristics, such as outstanding biodegradability and biocompatibility, good manufacturing practices, and cryopreservation properties.[26,27] There are few studies on the application of HES in stabilizing flavonoids NCs, nevertheless.

Luteolin (LUT), a flavonoid compound found in plants, such as celery and perilla leaves, has been proven to be beneficial for hyperuricemia (HUA) treatment.[6,28] In the present study, we demonstrate the feasibility of HES as the model stabilizer for preparing poorly soluble flavonoid NCs. The size and morphology of the prepared luteolin NCs (LUT-HES NCs), quercetin NCs (QUE-HES NCs), hesperidin NCs (HEP-HES NCs) and baicalin NCs (BAL-HES NCs) were characterized. Freeze-drying and storage stability of the LUT-HES NCs were tested without additional cryoprotectants. Saturated solubility, in vitro release, and cell uptake of LUT-HES NCs in intestinal epithelia-like Caco-2 cells were investigated. Finally, the in vivo pharmacokinetic profile and anti-hyperuricemic activity of the prepared LUT-HES NCs were evaluated in HUA mice.

## Materials and Methods

Luteolin (98.5%) was purchased from Must Biological Technology (Chengdu, China). HES (Mw: 200 KDa) was a gift from Hust Life Science and Technology (Wuhan, China). Diosmetin and quercetin (98%) were purchased from Herbest (Baoji, China). Baicalin (95%) was purchased from Solarbio (Beijing, China). Hesperidin (95%) was obtained from Yuanye Bio-Technology (Shanghai, China). Febuxostat (99%) was purchased from Harvey Bio (Beijing, China). Commercial assay kits for XO activity and blood biochemical analysis were purchased from Nanjing Jiancheng Bioengineering Institute (China). Dulbecco's modified Eagle's medium (DMEM), fetal bovine serum (FBS), non-essential amino acids, pancreatin and Hank's balanced salt solution (HBSS) were obtained from Gibco (USA). Other reagents were obtained from Sinopharm (Shanghai, China) or Thermo Fisher Scientific Inc. (USA).

Caco-2 cells were obtained from Immocell Biotechnology (Xiamen, China). Healthy male Sprague-Dawley (SD) rats (180 ± 20 g) and male ICR mice (18 ± 2 g) were provided by The Laboratory Animal Center of Hubei University of Medicine (Shiyan, China). The animals were raised according to the laws, rules, and guidelines for the care and use of laboratory animals. Food intake was restricted for 12 h prior to the experiment, and the animals were allowed to drink water freely.

### Preparation of Nanocrystals

The nanocrystals were produced by high-pressure homogenization (HPH). Briefly, HES was dissolved in 50 mL of ultrapure water, and a certain amount of luteolin was dispersed into the HES solution by high shearing (homogenizer PowerGen 125, Thermo Fisher Scientific, USA) at 13,000 rpm for 5 min. The coarse suspension was immediately

homogenized at 350 bar for six cycles and then further homogenized using a high-pressure homogenizer (EmulsiFlex-C3, Avestin, Canada) to obtain LUT-HES NCs. The LUT-HES NCs suspension was freeze-dried (LABCONCO, USA) and stored in a refrigerator at 4°C until further examination.

Luteolin concentration, LUT/HES weight ratio, homogenization pressure, temperature, and number of cycles are important technical parameters that affect the preparation of LUT-HES NCs. The average particle size, polydispersity index (PDI), zeta potential, and stability index (SI) were used as the investigation indices in this study, and the effects of these factors on the properties of the prepared LUT-HES NCs were investigated by single-factor experiments. The influencing factors and their values are presented in Table 1. When one factor was studied, the other factors were set as follows: drug concentration, 2 mg/mL; LUT/HES ratio (w/w), 1:1; homogenization pressure, 1000 bar; homogenization cycles, 20 times; homogenization temperature, 50°C. The stability of the LUT-HES NCs suspension was evaluated using the SI,[29] as shown in Equation (1):

$$SI = D_c/D_0 \times 100\% \quad (1)$$

where $D_0$ is the hydrated diameter of the LUT-HES NCs before centrifugation and $D_c$ is the corresponding hydrated diameter of LUT-HES NCs after centrifugation at 1500 rpm for 30 min. An SI value near 100% usually indicates that LUT-HES NCs are more stable.

## Characterization of Nanocrystals

### Dynamic Light Scattering

The hydrated diameter, PDI, and zeta potential of the nanocrystals were determined by dynamic light scattering (DLS) using a Zetasizer Nano ZS90 (Malvern Instruments, U.K.). Prior to testing, all the samples were diluted to an appropriate concentration using ultrapure water. The temperature was set at 25°C with an equilibrium time of 120 s. All measurements were performed in triplicate.

### Electron Microscopy

The shape and surface morphology analyses were carried out using scanning electron microscopy (SEM, Helios 5 CX, Thermo Scientific, USA) and transmission electron microscope (TEM, HT-7800, HITACHI, Japan).[30] An appropriate amount of drug coarse powder was evenly coated on the sample tank with the surface of the sample sprayed with gold, and the surface morphology was examined by SEM. Suspension of nanocrystals was applied to a copper grid for 30s and wicked off the excess amount of sample with filter paper prior to staining with phosphotungstic acid (1.5%) solution amidst repeated wicking off the stain solution. The morphology of the nanocrystals was observed by capturing an image of the resulting grid using TEM after air drying at room temperature.

### Drug Loading Efficiency and Drug Encapsulation Efficiency

Lyophilized LUT-HES NCs powder was resuspended in pure water and the suspension was diluted with acetonitrile, ultrasonicated to extract the luteolin.[31] After centrifugation (4°C, 12,000 rpm, 10 min), the concentration of luteolin was measured using a high-performance liquid chromatography (HPLC) system (Ultimate 3000, Thermo Fisher Scientific, USA) at 25°C. A Zorbax SB-$C_{18}$ column (250 mm × 4.60 mm, 5 μm, Agilent, USA) was used to separate the samples.

**Table 1** Factors Influencing the Preparation of LUT-HES NCs

| Experiments | Factors | Levels |
|---|---|---|
| 1 | Luteolin concentration (mg/mL) | 0.5, 1, 2, 5, 10 |
| 2 | LUT/HES ratio (w/w) | 1:3, 1:2, 1:1, 2:1 |
| 3 | Homogenization pressure (bar) | 400, 600, 800, 1000, 1200 |
| 4 | Homogenization cycles | 20, 30, 40, 50, 60 |
| 5 | Homogenization temperature (°C) | 30, 40, 50, 60, 70 |

**Abbreviations**: LUT, luteolin; HES, hydroxyethyl starch; NCs, nanocrystals; LUT-HES NCs, HES-stabilized LUT NCs.

The mobile phase consisted of a mixture of acetonitrile and water containing 0.2% phosphoric acid (volume ratio, 30:70) at a flow rate of 1 mL/min, and the injection volume was 10 μL. The UV detection wavelength was set to 350 nm. Drug loading efficiency (DLE) and drug encapsulation efficiency (DEE) were calculated using Equations (2) and (3):

$$DLE = \frac{weight\ of\ luteolin\ in\ the\ LUT-HES\ NCs\ sample}{weight\ of\ the\ LUT-HES\ NCs\ sample} \times 100\% \quad (2)$$

$$DEE = \frac{weight\ of\ luteolin\ in\ the\ LUT-HES\ NCs\ sample}{weight\ of\ the\ luteolin\ added} \times 100\% \quad (3)$$

### Re-dispersibility After Lyophilization

The re-dispersion capability of the prepared LUT-HES NCs after lyophilization was confirmed. The re-dispersibility index (RDI) was applied as the indicator.[29] The RDI was calculated using Equation (4):

$$RDI = D/D_0 \quad (4)$$

where $D_0$ represents the hydrated diameter of the freshly prepared LUT-HES NCs directly prior to solidification (lyophilization) and D represents the corresponding value of the reconstituted LUT-HES NCs after solidification. Therefore, an RDI of approximately 1 indicates that the LUT-HES NCs can be completely reconstituted after rehydration. The PDI and DLE of the LUT-HES NCs before and after freeze-drying were also determined to explore the physical stability of the prepared nanocrystals after lyophilization.

### X-Ray Diffraction

An X-ray diffractometer (Ultima IV, Rigaku, Japan) was used to determine the crystalline state of luteolin in LUT-HES NCs. The samples were subjected to Cu-Kα radiation (40 kV, 40 mA) at a scanning rate of 4°/min between 5 °and 45° with a step size of 0.02°.

### Fourier Transform-Infrared Spectrometer

The Fourier transform-infrared (FT-IR) spectra of LUT, HES, their physical mixture, and lyophilized LUT-HES NCs powder were obtained using an infrared spectrometer (Nicolet iS50, Thermo Scientific, USA).[32] The samples were prepared using a KBr standard. The obtained data were typically collected in the wavenumber range of 4000 to 400 $cm^{-1}$.

### Storage Stability

The storage stability of lyophilized LUT-HES NCs powder was investigated. The freeze-dried powder of LUT-HES NCs was stored at 4°C for nine months. At predetermined time points, the particle size, PDI, and drug content of the freeze-dried sample were determined after reconstitution in water.

### Saturated Solubility

The saturation solubility of luteolin was studied in ultrapure water. Briefly, excess luteolin, luteolin-HES physical mixture (LUT: HES = 1:1, w/w), and LUT-HES NCs freeze-dried powder were added to 5 mL ultrapure water respectively and then incubated at 37°C with shaking for 24 h. The undissolved drug was removed by centrifugation at 12,000 rpm for 30 min and filtered through a syringe filter (0.22 μm), and the drug concentration in the filtrate was determined by HPLC.

### In vitro Dissolution

The in vitro release of the bulk drug and nanocrystal formulation was evaluated using the paddle method, according to the China Pharmacopoeia 2020. In brief, 2.5 mg (luteolin) of luteolin coarse drug mixed with HES or LUT-HES NCs was added to 500 mL of simulated gastric fluid (SGF, pH 1.2 HCl containing 0.5% Tween 80) or simulated intestinal fluid (SIF, pH 6.8 buffer salt solution containing 0.5% Tween 80). The speed was 100 rpm, and the temperature was set to 37.0 ± 0.5°C. Approximately 4 mL of the sample solution was withdrawn periodically and immediately filtered through a 0.22 μm syringe filter. An equal volume of fresh dissolution medium was then added to maintain a constant volume. The samples were quantitatively analyzed by HPLC. Dissolution studies were performed in triplicate.

## Cellular Uptake and Mechanisms

The cellular uptake of LUT-HES NCs was investigated in a Caco-2 cell monolayer model as previously reported.[33] In brief, Caco-2 cells were seeded onto 24-well plates at a density of $2.5\times10^4$ cells/cell and cultured for 14 days. Prior to the study, the cells were rinsed with pre-warmed HBSS (37°C). The cells were incubated with 1 mL of LUT solution (dissolved in HBSS with 0.1% DMSO), physical mixture solution of LUT and HES (dissolved in HBSS with 0.1% DMSO), and LUT-HES NCs suspension dispersed in HBSS at 37°C for 4 h, respectively. Three formulations were prepared at a luteolin concentration of 30 μM. After incubation, the cells were washed three times with PBS and cell lysis was performed by ultrasonication. Luteolin content of the lysate was analyzed using HPLC. Cellular protein concentration in the lysate was measured using the BCA kit. The cellular uptake of luteolin was expressed as the amount of luteolin associated with 1 mg of cellular protein.

To explore the mechanism of cellular internalization, Caco-2 cells were treated with inhibitors of various endocytic pathways. Prior to experiment of cellular uptake, Caco-2 cells were pretreated with chlorpromazine (30μmol/L), colchicine (4 μg/mL), indomethacin (50 μg /mL), or sodium azide (650 μg /mL) in 1 mL of HBSS at 37°C for 1 h, respectively. Cells treated with a cell culture medium without inhibitors were used as controls. Subsequently, the LUT solution and LUT-HES NCs suspension were added to the cells after rinsing with HBSS. Cellular uptake experiments were conducted according to the protocol described above. The amount of luteolin internalized by inhibitor-treated cells was compared to that in the control group.

## Pharmacokinetics in Rats

The pharmacokinetics of luteolin was investigated in SD rats. Twelve male SD rats were randomly divided into two groups (n = 6). (1) LUT group: luteolin coarse drug dispersed in normal saline; (2) LUT-HES NCs group: LUT-HES NCs suspension in normal saline. After the rats were fasted for 12 h, the two formulations were respectively given to the rats in the two groups via gavage at a luteolin dose of 30 mg/kg. Blood samples (approximately 0.5 mL) were collected via retro-orbital puncture at predetermined intervals (0.25, 0.5, 1, 2, 4, 8, 12, and 24 h) and then centrifuged at 4000 rpm for 10 min to obtain plasma. The obtained plasma samples were stored at −80°C until analysis.

A liquid–liquid extraction method was used to extract luteolin from the plasma samples and the processing methods were as follows. In brief, 10 μL of diosmetin solution (0.3 μg/mL, internal standard), 100 μL of 6% perchloric acid-methanol solution, and chloroform (1.5 mL) were added to a 100 μL aliquot of the plasma sample. After vortexing for 5 min and centrifugation at 3500 rpm for 10 min, the supernatant was collected and dried at room temperature under a gentle stream of nitrogen. The dried residue was reconstituted in 100 μL of a mixture of acetonitrile and water containing 0.2% phosphoric acid (volume ratio, 30:70) followed by centrifugation (12,000 rpm, 10 min) for the luteolin assay. The processed samples (2 μL) were injected into a HPLC-MS/MS system (TSQ Quantiva, Thermo Fisher Scientific, USA). Chromatographic separation of the sample was performed using an ACQUITY UPLC BEH $C_{18}$ Column (1.7 μm, 2.1×50 mm, Waters, USA) at 40°C. The mobile phase was a mixture of methanol (A) and water containing 0.2% phosphoric acid (B) at 0.2 mL/min. The following linear gradient was used: started at 45% A, increased to 70% A over 2 min, increased to 100% A over 0.1 min, hold at 100% A over 2.9 min, then returned to initial conditions over 0.1 min and re-equilibrated for 2.9 min. Luteolin and diosmetin were analyzed in negative ionization mode and detected by multiple reaction monitoring for the transition of precursor ions: luteolin (m/z 285>133) and diosmetin (m/z 301>258). Luteolin concentration in plasma samples was calculated using the internal standard method.

The concentration-time curve of luteolin after administration was recorded, and the main pharmacokinetic parameters were calculated using Drug and Statistics (DAS) software (version 2.0, Mathematical Pharmacology Professional Committee of China, Shanghai, China). The pharmacokinetic parameters were obtained via non-compartmental analysis of the data. Likewise, the oral relative bioavailability (Fr) of LUT-HES NCs was calculated using Equation (5):

$$Fr = \frac{AUC_T}{AUC_R} \times 100\% \tag{5}$$

Where $AUC_T$ and $AUC_R$ are the areas under the concentration-time curves of LUT-HES NCs and free LUT, respectively.

### In vivo Studies Using Mice Model

Forty-eight male ICR mice were randomly assigned to six groups (n = 8). (1) control group-1: normal mice treated with normal saline; (2) control group-2: normal mice treated with LUT-HES NCs (suspended in normal saline, equivalent to 30 mg/kg of luteolin); (3) HUA model group: HUA model mice treated with normal saline; (4) febuxostat group: HUA model mice treated with febuxostat (positive drug, dispersed in normal saline, 10 mg/kg); (5) LUT group: HUA model mice treated with luteolin coarse drug (dispersed in normal saline, 30 mg/kg); (6) LUT-HES NCs group: HUA model mice treated with LUT-HES NCs (equivalent to 30 mg/kg of luteolin). The HUA model mice were induced via the intraperitoneally injected with oxonic acid potassium (PO, 300 mg/kg) and hypoxanthine (HX, 300 mg/kg) suspension (dispersed in normal saline) for seven consecutive days. Accordingly, the two control groups were intraperitoneally administered the same amount of normal saline by intraperitoneal injection.

To evaluate the in vivo efficacy of LUT-HES NCs against HUA, luteolin formulations were administered orally for 2 weeks, including a 1-week pretreatment. Accordingly, the two control groups and the HUA group were administered the same amount of normal saline via gavage. Febuxostat was administered orally as a positive control for one week. The animals were euthanized at the end of the 14 days' treatment period. Blood samples were collected for biochemical analyses. Different organs (the heart, liver, spleen, lungs, and kidneys) were excised immediately and carefully after blood collection. The kidneys were weighed, and the renal index ($weight_{kidney}/weight_{mice} \times 100\%$) was calculated. Serum uric acid, serum xanthine oxidase (XO) activity, hepatic XO activity, serum creatinine (SCr), blood urea nitrogen (BUN), aspartate aminotransferase (AST), and alanine aminotransferase (ALT) levels were measured using commercial assay kits. Urate transport protein 1 (URAT1) and Glucose Transporter 9 (GLUT9) in the kidney tissues were analyzed by Western blotting. The organs were then fixed with 4% paraformaldehyde for hematoxylin and eosin (H&E) staining.

## Statistical Analysis

Results are reported as the mean ± standard deviation or mean ± standard error of the given number of independent experiments. Statistical analysis was performed by one-way analysis of variance using SPSS statistical software. Differences were considered statistically significant at $P$ value < 0.05.

# Results and Discussion

## Preparation, Optimization and Characterization

This study aimed to evaluate the potential of HES as a natural stabilizer for poorly soluble flavonoid NCs. The feasibility of HES as the stabilizer for preparing LUT NCs (LUT-HES NCs) was firstly verified using the "top-down" principle by HPH technique. The techniques applied to prepare nanosuspensions include homogenization, milling and precipitation.[34] In the present study, homogenization, commonly used in the commercial production of nanocrystals formulations, was selected because it could be easily scaled up with good reproducibility.[15] The effects of luteolin concentration, LUT/HES weight ratio, homogenization pressure, temperature and circles on the properties of LUT-HES NCs were investigated by the single-factor test.

The average particle size of the LUT-HES NCs decreased as the LUT content increased from 0.5 to 5 mg/mL ($P$<0.001) and did not change significantly when the LUT concentration increased to 10 mg/mL. Within the experimental range, the PDI showed negligible alterations (Figure 1A and F). Unfortunately, blockage of the feeding port of the instrument was observed at a drug concentration of 10 mg/mL. Given the preparation efficiency and equipment damage, the optimal LUT concentration of 5 mg/mL was selected.

Similarly, the LUT/HES weight ratio did not affect the uniformity of the prepared nanosuspension in our experimental range, whereas the smallest particle size (~ 240 nm) was obtained when the LUT/HES weight ratio was 1:1 (Figure 1B and G). When the HES concentration was lower than the optimal concentration, the surface of the nanocrystals was incompletely covered by the stabilizer, resulting in the aggregation and growth of the particles. A further increase in the amount of HES resulted in an increase in the particle size ($P$<0.001), which might result from the thickened stabilizer layer coating the surface of the LUT-HES NCs. HES is an amphiphilic biopolymer that contains a large amount of hydroxyl groups, providing opportunities for adequate drug binding.[22] Hydrogen bonds could be formed between the hydroxyl functional groups in HES and the phenolic hydroxyl groups in flavonoids.[19] Therefore, HES could adhere to the

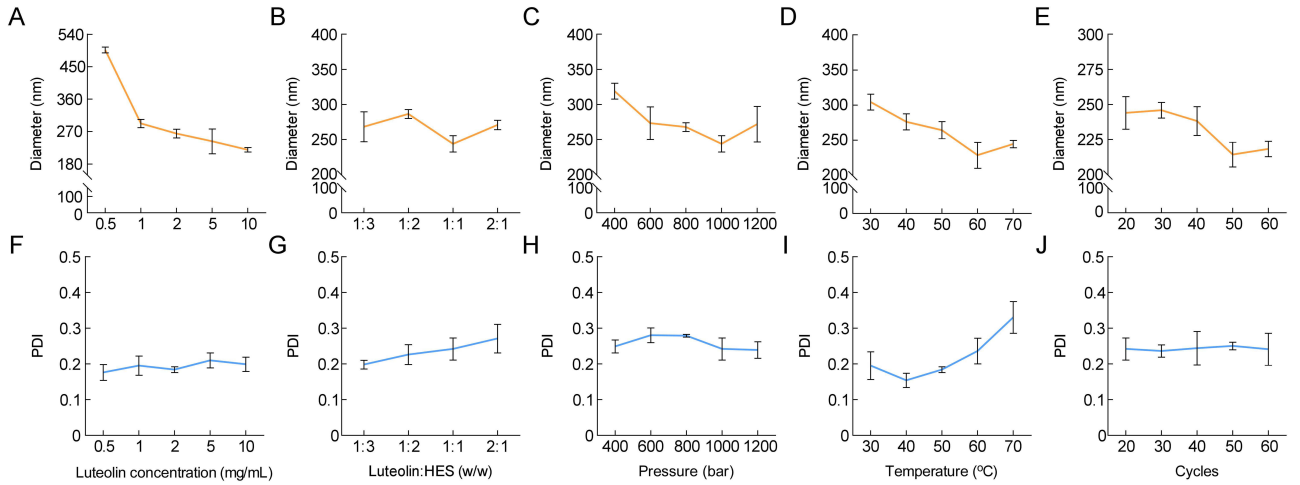


**Figure 1** The effect of luteolin concentration (**A** and **F**), LUT/HES weight ratio (**B** and **G**), homogenization pressure (**C** and **H**), homogenization temperature (**D** and **I**) and homogenization cycles (**E** and **J**) on size distribution of the prepared LUT-HES NCs.
**Note**: Data are reported as mean ± SD, n=3.
**Abbreviations**: LUT, luteolin; HES, hydroxyethyl starch; NCs, nanocrystals; LUT-HES NCs, HES-stabilized LUT NCs; PDI, polydispersity index.

surface of luteolin by hydrogen bonding and hydrophobic forces to generate steric resistance between particles. At the same time, the hydrophilic part of HES extends into the aqueous dispersion medium to form a thicker hydration film, thereby enhancing steric stabilization and preventing the agglomeration of particles. However, the effect of the amount of polymer compound on nanosuspensions was complicated.[35] Enough polymer was needed to cover the surface of the particles for stability. Whereas excess polymer did not protect them from aggregation, but rather made the polymer chain play a "bridge" role, which led to aggregation and even deposition of the particles.[18]

The particle size decreased ($P<0.01$) with an increase in the homogenization pressure (400–1000 bar), and a higher operating pressure did not cause a further reduction in the particle size (Figure 1C). The PDI of the LUT-HES NCs was also affected. No significant change in the PDI could be obtained when the pressure was less than 800 bar. When the homogenization pressure increased from 800 to 1000 bar, the PDI decreased ($P<0.01$), and no obvious fading was observed when the pressure continued to increase to 1200 bar (Figure 1H). Therefore, the optimal homogenization pressure was determined to be 1000 bar, and the prepared LUT-HES NCs exhibited the smallest particle size (244 nm) and PDI (0.242).

When the homogenization temperature increased from 30°C to 60°C, the particle size decreased ($P<0.01$), and further increase in temperature resulted in no significant alteration in particle size (Figure 1D). The PDI was not noticeably affected by the homogenization temperatures below 50°C, but it remarkably increased when the temperature expanded to 70°C ($P<0.01$) (Figure 1I). Considering the energy consumption during preparation, 50°C was selected as the optimal homogenization temperature.

Homogenization cycles did not significantly influence the particle size of the LUT-HES NCs when the number was less than 40 (Figure 1E). Increasing the circle number to 50 led to a distinct reduction in the particle size ($P<0.05$). However, when it increased from 50 to 60, the particle size remained nearly unchanged ($P>0.05$). Number of cycles do not significantly affect the uniformity of the prepared nanosuspensions within the experimental range (Figure 1J). Hence, the optimal homogenization cycle number was determined to be 50.

According to the results of the above study, all factors could influence the size distribution of LUT-HES NCs, whereas the zeta potential and SI were slightly influenced (Figure S1). The surface zeta potential of the LUT-HES NCs ranged from −20 to −25 mV, which could be attributed to the same stabilizer coating on the surface of the LUT NCs. In addition, the SI was approximately 100%, indicating the high stability of the prepared LUT-HES NCs suspensions.

Taken together, the optimum parameters for luteolin concentration, LUT/HES weight ratio, homogenization pressure, temperature, and cycles for LUT-HES NCs preparation were 5 mg/mL, 1:1, 1000 bar, 50°C, and 50, respectively. The optimized LUT-HES NCs were fully characterized (Figure 2). The average particle size was 191.1 ± 16.8 nm and the PDI was approximately 0.239, demonstrating the relatively beneficial homogeneity of the LUT-HES NCs (Figure 2B). Coarse luteolin

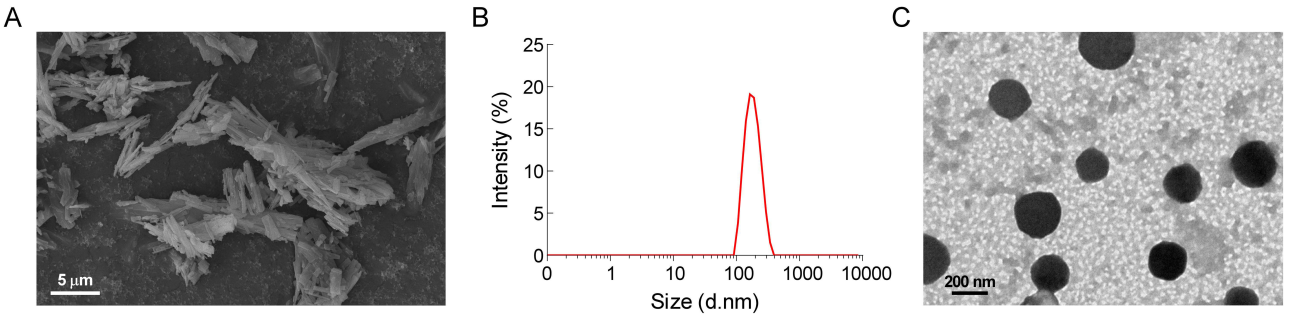


**Figure 2** Representative SEM image of luteolin coarse crystal (**A**), size distribution (**B**) and representative TEM image (**C**) of LUT-HES NCs.
**Note**: Size distribution of LUT-HES NCs was determined using by DLS using a Zetasizer Nano ZS90.
**Abbreviations**: SEM, scanning electron microscopy; TEM, transmission electron microscopy; LUT, luteolin; HES, hydroxyethyl starch; NCs, nanocrystals; LUT-HES NCs, HES-stabilized LUT NCs; DLS, dynamic light scattering.

was a virgulate crystal with a diameter of tens of microns and an uneven size distribution (Figure 2A), whereas the LUT-HES NCs were nearly spherical with a smooth outer surface and uniform dispersion (Figure 2C). The zeta potential was approximately −23 mV (data not shown), indicating that electrostatic repulsion existed in the LUT-HES NCs. Meanwhile, high drug-loading efficiency (49.26 ± 0.50%) and drug encapsulation efficiency (98.52 ± 1.01%) were achieved. Besides, HES-stabilized LUT NCs were obtained through bottom-up technology using a precipitation method as well (Figure S2). Furthermore, flavonoid NCs such as quercetin NCs, hesperidin NCs, and baicalin NCs stabilized by HES were successfully prepared (Figure S3). These results support the application of HES as a stabilizer for the preparation of various poorly soluble flavonoid NCs.

## Freeze-Drying

The re-dispersibility studies were carried out to confirm the role of HES as a cryoprotectant to solidify LUT-HES NCs. HES has been clinically used as a non-penetrating cryoprotectant for cell, tissue, and organ storage.[22] It exhibits the ability to absorb water molecules and remain thermally inert in a glassy state without experiencing any phase transition during cooling.[27] The data showed only a slight increase in the size and PDI of LUT-HES NCs after freeze-drying, and almost no change in the drug content was observed (Table 2). The slight aggregation of lyophilized LUT-HES NCs could be caused by the possible polymer-chain entanglement of HES during lyophilization, which did not impair the re-dispersibility of the LUT-HES NCs. These results indicate that HES is a prominent stabilizer of LUT NCs and plays a distinct role in protecting the LUT-HES NCs from irreversible agglomeration during freeze-drying.

## Crystalline State

Crystalline state is one of the most important factors affecting drug stability, solubility, and efficacy.[18] The crystal state of LUT was studied using XRD. Figure 3A shows the XRD spectra of different samples. The XRD patterns of the LUT-HES NCs and the physical mixture were consistent with those of LUT, revealing that the crystalline state of LUT did not change significantly during preparation and freeze-drying. The intensity of the diffraction peaks in LUT-HES NCs was significantly lower than that of the LUT and physical mixture. It could be explained by the decrease in drug particle size leading to a signal reduction in crystallinity.[18,36]

**Table 2** Size Distribution and DLE of LUT-HES NCs Before and After Lyophilization

| | Diameter (nm) | PDI | RDI | DLE (%) |
|---|---|---|---|---|
| Before | 191.1 ± 16.8 | 0.251 ± 0.004 | – | 48.38 ± 1.00 |
| After | 222.3 ± 3.4 | 0.285 ± 0.007 | 1.16 | 48.43 ± 1.46 |

**Notes**: Data are reported as mean ± SD, n=3. RDI, the proportion of the hydrated diameter of LUT-HES NCs before and after lyophilization.
**Abbreviations**: LUT, luteolin; HES, hydroxyethyl starch; NCs, nanocrystals; LUT-HES NCs, HES-stabilized LUT NCs; PDI, polydispersity index; RDI, re-dispersibility index; DLE, drug loading efficiency.

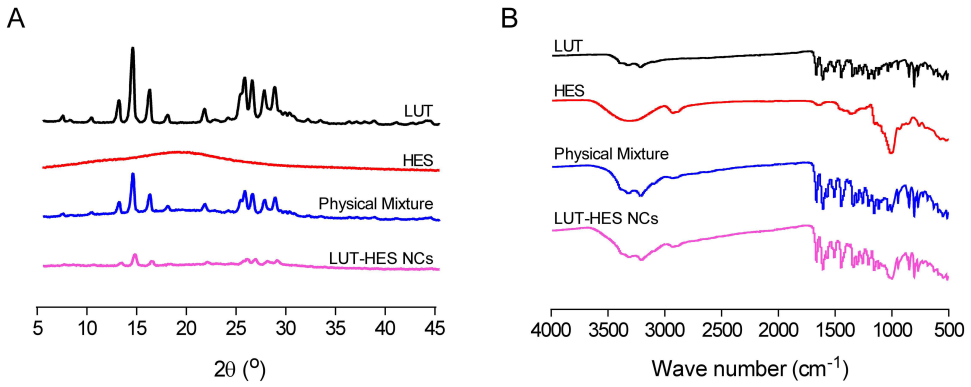


**Figure 3** The XRD (**A**) and FT-IR spectra (**B**) of LUT, HES, their physical mixture, and lyophilized LUT-HES NCs powder.
**Abbreviations**: XRD, X-Ray Diffraction; FT-IR, Fourier transform-infrared; LUT, luteolin; HES, hydroxyethyl starch; NCs, nanocrystals; LUT-HES NCs, HES-stabilized LUT NCs.

## Chemical Structure

FT-IR analysis was conducted to determine the chemical structure of LUT-HES NCs. The infrared spectra of the LUT coarse crystal, HES, physical mixture, and LUT-HES NCs are shown in Figure 3B. Characteristic peaks of LUT coarse drugs were observed at 3319 $cm^{-1}$, 3211 $cm^{-1}$, 1662 $cm^{-1}$, 1608 $cm^{-1}$, 1505 $cm^{-1}$ and 1444 $cm^{-1}$, which were ascribed to functional groups such as phenolic hydroxyl, C=C, C=O, and aromatic rings of luteolin.[13,37] The spectrum of HES exhibited some characteristic absorption peaks at 3298 $cm^{-1}$, 2924 $cm^{-1}$, 1359 $cm^{-1}$, and 998 $cm^{-1}$, which correspond to O-H stretching vibrations, C-H stretching vibration, O-H bending vibration, and C-O stretching vibration, respectively.[24] All the peaks of LUT-HES NCs were found in the infrared spectra of HES and LUT, indicating that no covalent bond existed between HES and LUT. The absorption peak of the LUT-HES NCs was not the same as that of the physical mixture, probably because of the HES coating on the surface of the LUT-HES NCs. In addition, the characteristic peak of the phenolic hydroxyl in the spectrum of LUT-HES NCs shifted from 3211 $cm^{-1}$ to 3203 $cm^{-1}$, which may be due to the mutual interaction between the phenolic hydroxyl in LUT and the hydroxyl in HES.[18,37]

## Storage Stability

To verify whether the properties of LUT-HES NCs has changed with prolonged storage time, lyophilized LUT-HES NCs powder was stored at 4°C for nine months. From Figure 4, we can conclude that mild fluctuations in the particle size and PDI were observed. The alteration in drug concentration was less than 5% during nine months of storage, demonstrating that slight chemical degradation of LUT occurred after long storage. The particle size was slightly increased, which could be explicated by the fact that there was a large surface energy between the nano-sized particles.[38] To improve the thermodynamic stability, the nanoparticles tended to aggregate, resulting in a slight increase in the particle size. The above results revealed that the optimized LUT-HES NCs formulation was physically and chemically stable, with a shelf life of at least nine months, which could be due to the presence of the stabilizer. HES allowed the LUT-HES NCs to be evenly dispersed, preventing the agglomeration of the particles and guaranteeing the stability of the formulation.

## Saturation Solubility and in vitro Dissolution Studies

Figure 5 demonstrated the saturation solubility of coarse drug powder and the LUT-HES NCs freeze-dried powder in distilled water. The saturation solubility of LUT and LUT-HES NCs were 0.94 ± 0.07 and 7.04 ± 0.06 μg/mL, respectively. The solubility of LUT-HES NCs was 7.49 times the value of LUT ($P<0.001$), contributed most by nano-size of LUT-HES NCs, which could be explained by the Ostwald–Freundlich equation.[14,39]

The in vitro dissolution of LUT powder and freeze-dried LUT-HES NCs powder was organized in simulated gastric and intestinal fluids. The in vitro dissolution curves are shown in Figure 6. Within 3 min, approximately 93.67% and 87.50% of the drug was dissolved from the freeze-dried LUT-HES NCs in the SGF and SIF, respectively. In contrast, the cumulative dissolution for LUT was only 25.78% and 48.47% in the two media. According to the Noyes-Whitney equation, drug dissolution rate is

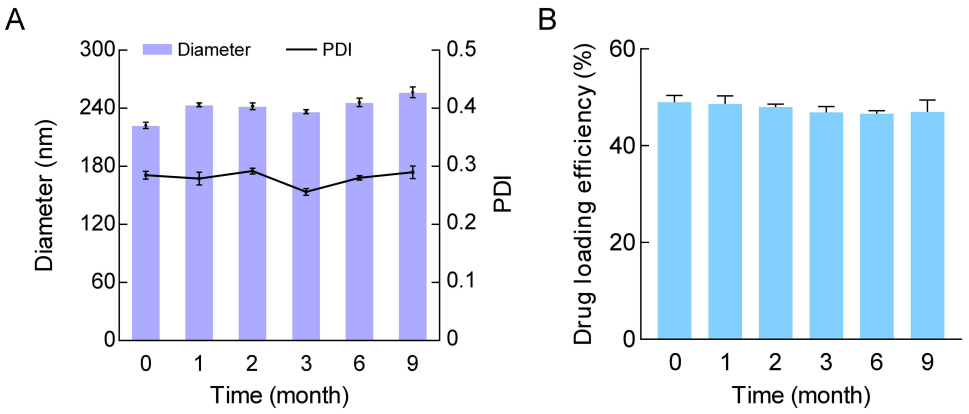


**Figure 4** The average size and PDI (**A**) and DLE (**B**) of lyophilized LUT-HES NCs powder during storage.
**Notes**: Samples were stored at 4° and analyzed after reconstitution in water at predetermined time points. Data are reported as mean ± SD, n=3.
**Abbreviations**: DLE, drug loading efficiency; LUT, luteolin; HES, hydroxyethyl starch; NCs, nanocrystals; LUT-HES NCs, HES-stabilized LUT NCs; PDI, polydispersity index.

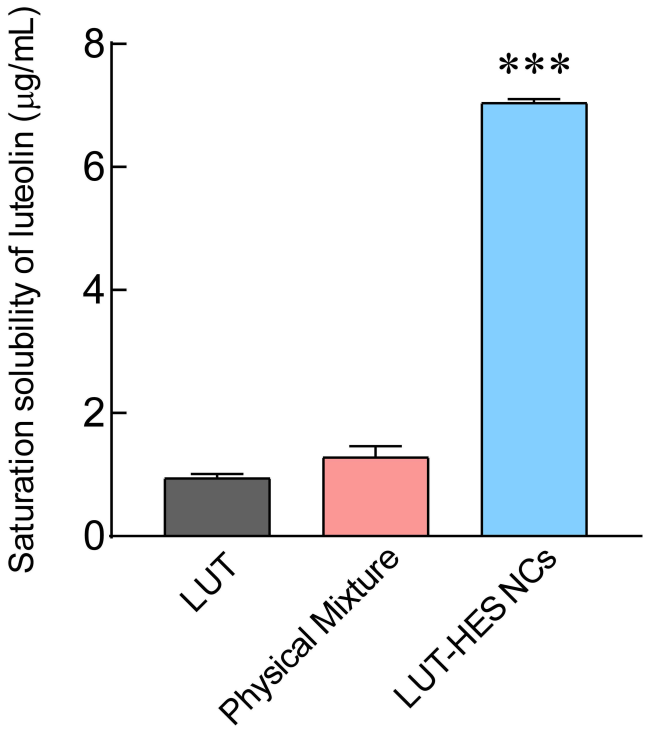


**Figure 5** The saturation solubility of different formulations (LUT, physical mixture and LUT-HES NCs) in water.
**Notes**: Excess samples were added to 5 mL ultrapure water and incubated at 37°C with shaking for 24 h. The undissolved drug was removed by centrifugation and filtration. The drug concentration in the filtrate was determined by HPLC. Data are reported as mean ± SD, n=3. ***$P<0.001$, compared to the LUT group.
**Abbreviations**: LUT, luteolin; HES, hydroxyethyl starch; NCs, nanocrystals; LUT-HES NCs, HES-stabilized LUT NCs.

proportional to the special surface area.[14] LUT-HES NCs dissolve easily into the gastrointestinal fluid because they have a greater surface area than coarse crystalline drugs under equivalent conditions. We can conclude that particle size reduction lead to an enhanced dissolution velocity of LUT-HES NCs. These results revealed that the LUT-HES NCs formulation could remarkably improve the saturation solubility and dissolution rate, which might be beneficial to the bioavailability of luteolin.

## Cellular Uptake in Caco-2 Cells

The Caco-2 cell model is most commonly used to evaluate in vitro intestinal permeability of compounds.[40] A cytotoxicity study was conducted to explore the influence of different luteolin formulations on the viability of Caco-2 cells. The LUT

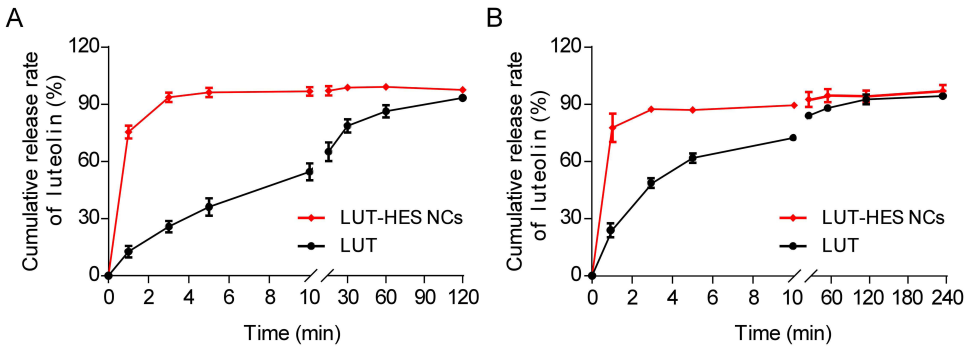


**Figure 6** In vitro dissolution of luteolin from free LUT and LUT-HES NCs in SGF (**A**) and SIF (**B**) using the paddle method.
**Notes**: Data are reported as mean ± SD, n=3. SGF: pH 1.2 HCl containing 0.5% Tween 80; SIF: pH 6.8 buffer salt solution containing 0.5% Tween 80.
**Abbreviations**: SGF, simulated gastric fluid; SIF, simulated intestinal fluid; LUT, luteolin; HES, hydroxyethyl starch; NCs, nanocrystals; LUT-HES NCs, HES-stabilized LUT NCs.

solution, a physical mixture solution (LUT and HES), and LUT-HES NCs suspensions, did not affect the viability of Caco-2 cells under the experimental conditions (Figure S4).

As presented in Figure 7A, the amount of cellular uptake of the LUT-HES NCs group was 71.85 ± 9.66 μg luteolin/mg cellular protein, which was significantly higher than that of free LUT (25.89 ± 4.94 μg luteolin/mg cellular protein). It revealed that LUT-HES NCs significantly improved the intestinal absorption of luteolin. In addition, there was no significant difference between the physical mixture and LUT groups, indicating that HES itself did not affect the intestinal permeability of the drug. NCs are generally assumed to dissolve more than coarse drugs, thus forming a higher drug concentration gradient and leading to enhanced absorption in the gastrointestinal tract.[14] However, luteolin in the physical mixture and LUT groups was dissolved in this study. Our results supported that NCs could further improve the absorption of poorly soluble drugs through other absorption mechanisms, such as the endocytosis pathway.[14,41,42] To characterize the molecular mechanisms underlying the endocytic pathway in Caco-2 cells, we examined the effects of inhibitors of different endocytosis pathways on the uptake of LUT and LUT-HES NCs.

In cells treated with LUT solution, the cellular uptake of luteolin significantly reduced after incubation with sodium azide (Figure 7B). This suggests that the cellular internalization of luteolin in Caco-2 cells is energy dependent. To date, a few reports have revealed that the uptake of flavonoids in Caco-2 cells is energy dependent,[43,44] but the endocytosis pathway involved remains unclear. As shown in Figure 7B, no significant change was observed in the cellular uptake

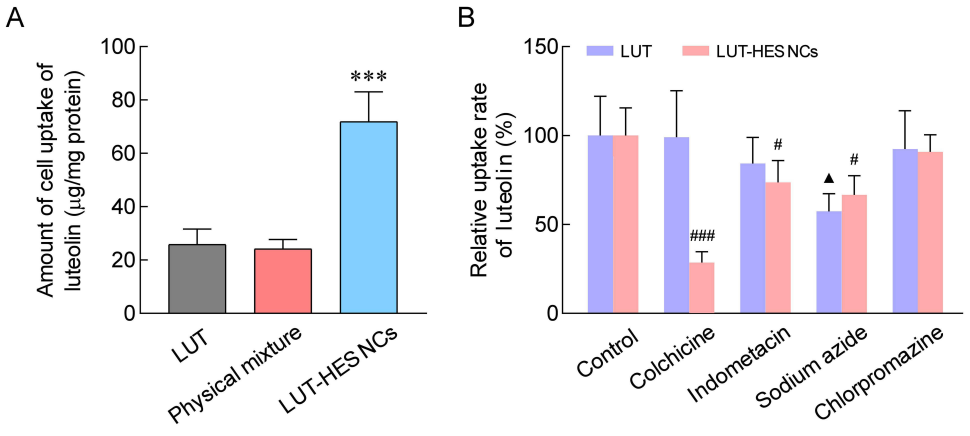


**Figure 7** Cellular uptake of LUT-HES NCs in Caco-2 cells: (**A**) The cellular uptake of LUT, physical mixture and LUT-HES NCs in Caco-2 cells; (**B**) Cell uptake efficiency of LUT and LUT-HES NCs with inhibitors including chlorpromazine, indomethacin, sodium azide and colchicine.
**Notes**: The cell uptake of LUT or LUT-HES NCs without any treatment was served as control, respectively. Data are reported as mean ± SD, n=4. ***$P<0.001$, compared to the LUT group. ▲$P<0.05$, compared to the LUT control group; #$P<0.05$, ###$P<0.001$, compared to the LUT-HES NCs control group.
**Abbreviations**: LUT, luteolin; HES, hydroxyethyl starch; NCs, nanocrystals; LUT-HES NCs, HES-stabilized LUT NCs.

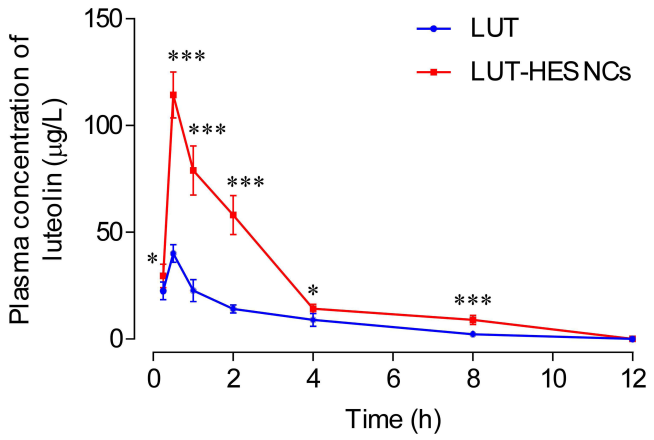


**Figure 8** Plasma concentration-time diagram of free LUT and LUT-HES NCs in rats after oral administration at a luteolin dose of 30 mg/kg.
**Note**: Data are reported as mean ± SD, n=6. *$P$<0.05, ***$P$<0.001, compared to LUT group.
**Abbreviations**: LUT, luteolin; HES, hydroxyethyl starch; NCs, nanocrystals; LUT-HES NCs, HES-stabilized LUT NCs.

after treatment with chlorpromazine, indomethacin, or colchicine, indicating that clathrin-mediated endocytosis, caveolae-mediated endocytosis, and micropinocytosis did not participate in free luteolin internalization in Caco-2 cells.

Comparatively, chlorpromazine did not affect the uptake of LUT-HES NCs by inhibiting clathrin-mediated endocytosis, whereas colchicine, indomethacin, and sodium azide resulted in 71.8%, 26.8%, and 33.8% reductions in cellular uptake, respectively (Figure 7B). This indicated that the cellular uptake of LUT-HES NCs was energy-dependent, and that LUT-HES NCs could be internalized into enterocytes via micropinocytosis and caveolae-mediated endocytosis. It could be concluded from the above results that LUT-HES NCs changed the endocytosis pathway of luteolin, which might be the main reason for the enhanced intestinal absorption of luteolin by LUT-HES NCs.

## Pharmacokinetic Studies in Rats

To confirm the advantage of LUT-HES NCs in improving drug bioavailability, in vivo pharmacokinetic studies were performed in rats. The plasma concentration-time curves of the luteolin coarse suspension (LUT) and LUT-HES NCs were displayed in Figure 8, and the pharmacokinetic parameters were shown in Table 3. After oral administration, the two luteolin formulations showed similar concentration-time dependent curve. However, the plasma concentration of LUT-HES NCs was higher than that of free LUT at different time points. The $AUC_{0\text{-}\infty}$ of free LUT and LUT-HES NCs groups were 98.6 ± 26.7 and 350.7 ± 34.1 μg/L·h, respectively. It demonstrated that LUT-HES NCs remarkably increased the bioavailability of luteolin with a relative oral bioavailability of 355.7%. Based on previous studies in this paper, improved bioavailability by LUT-HES NCs can be attributed to increased saturation solubility, drug dissolution rate, and intestinal uptake of luteolin.

**Table 3** Main Pharmacokinetic Parameters of Free LUT and LUT-HES NCs in Rats

| Parameters | LUT | LUT-HES NCs |
|---|---|---|
| $C_{max}$ (μg/L) | 40.1 ± 4.5 | 114.4 ± 11.8*** |
| $T_{max}$ (h) | 0.5 ± 0.0 | 0.5 ± 0.0 |
| $t_{1/2}$ (h) | 2.2 ± 0.6 | 2.2 ± 0.2 |
| $AUC_{0\text{-}\infty}$ (μg/L·h) | 98.6 ± 26.7 | 350.7 ± 34.1*** |
| Fr (%) | – | 355.7 |

**Note**: Data are reported as mean ± SD, n=6. ***$P$<0.001, compared with free LUT group.
**Abbreviations**: LUT, luteolin; HES, hydroxyethyl starch; NCs, nanocrystals; LUT-HES NCs, HES-stabilized LUT NCs; $C_{max}$, peak concentration; $T_{max}$, time to reach $C_{max}$; $t_{1/2}$, half-life; *AUC*, area under the curve; Fr, relative bioavailability.

## Pharmacodynamic Studies Using Mice Model

An in vivo anti-hyperuricemia study of LUT-HES NCs was performed using the HUA mice model, and febuxostat was chosen as the positive control group because of its broad clinical application in HUA treatment (Figure 9A).[45] As shown in Figure 9B, the mean serum UA level of the model group (781.33 ± 34.71 μmol/L) was significantly higher than that of the normal control group, indicating that the HUA mouse model was successfully established.[46] At the same time, it was found that the serum UA levels were reduced by 51.67% by free LUT and 69.93% by the LUT-HES NCs compared with the HUA group. At the same dose, the decrease in UA level in the LUT-HES NCs group was significantly greater than that in the LUT group ($P$<0.01). The mechanisms by which LUT-HES NCs exhibited enhanced urate-lowering effect were also explored. As shown in Figure 9C–F, LUT-HES

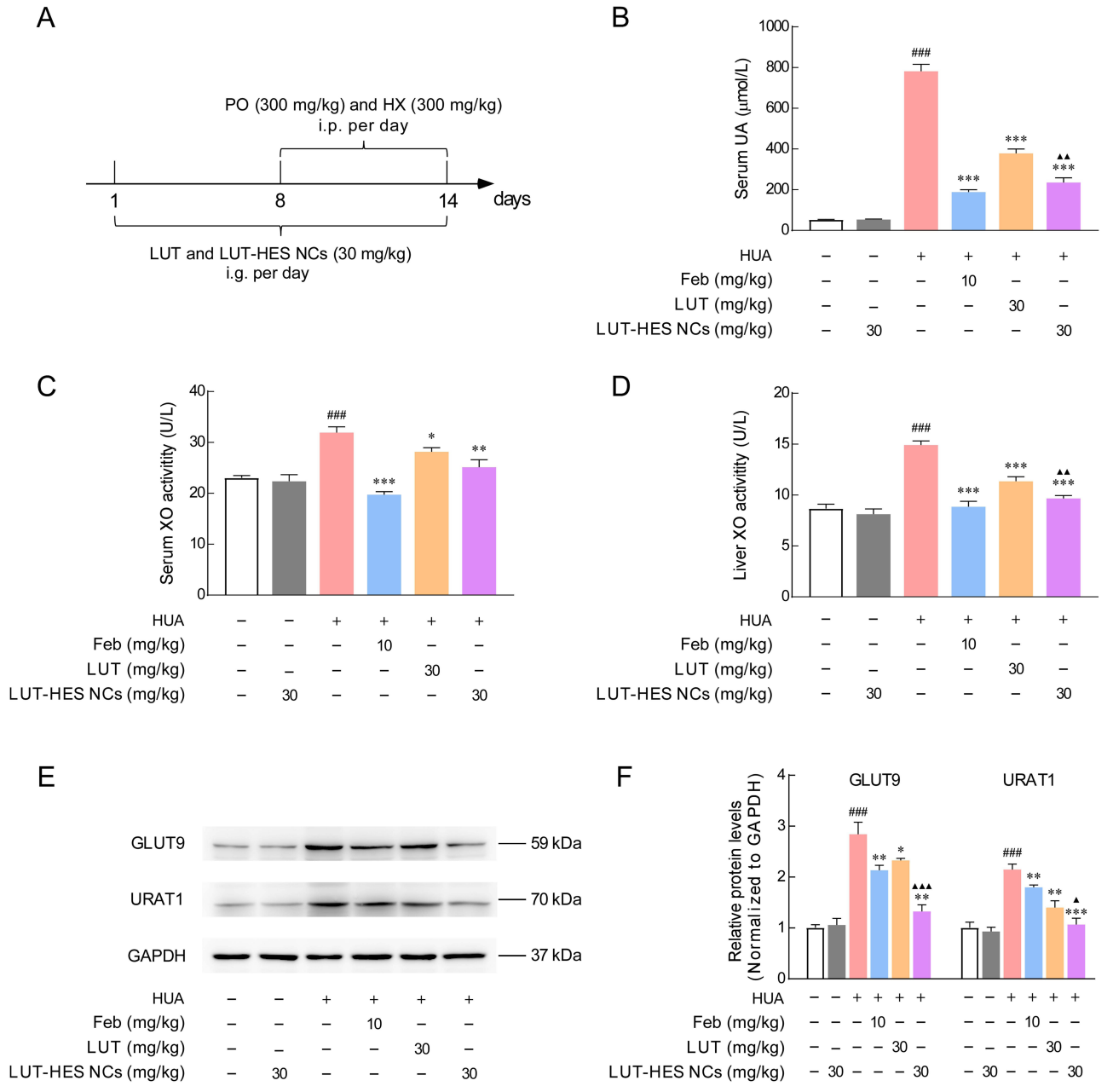


**Figure 9** Urate-lowering efficacy of LUT-HES NCs on HUA mice: (**A**) Schematic illustration of the establishment of HUA mice model and dosing regimen; (**B**) Serum UA; (**C** and **D**) serum and hepatic XO activity; (**E** and **F**) protein expression of GLUT9 and URAT1 in the renal tissues by Western blotting.

**Notes**: Data are reported as mean ± SEM, n=8. ###$P$<0.001, versus the control group; *$P$<0.05, **$P$<0.01, ***$P$<0.001, versus the model group; ▲$P$<0.05, ▲▲$P$<0.01, ▲▲▲$P$<0.001, versus the LUT group.

**Abbreviations**: LUT, luteolin; HES, hydroxyethyl starch; NCs, nanocrystals; LUT-HES NCs, HES-stabilized LUT NCs; Feb, febuxostat; HUA, hyperuricemia; PO, oxonic acid potassium; HX, hypoxanthine; UA, uric acid; XO, xanthine oxidase; GLUT9, Glucose Transporter 9; URAT1, urate transport protein 1.

NCs treatment more effectively inhibited XO activity (both in serum and in the liver) and promoted urate excretion compared to LUT. In summary, these results suggested that LUT-HES NCs dramatically improved the activity of LUT against hyperuricemia by reducing urate production and increasing urate excretion.

Hyperuricemia is associated with tissue damage, particularly with renal injury.[47] To investigate the protective effect of LUT-HES NCs on multiple organs of HUA mice, the renal index, hepatic and renal function, and histological examination were performed (Figures 10 and 11). The kidneys in the HUA model group displayed pathological changes such as swelling

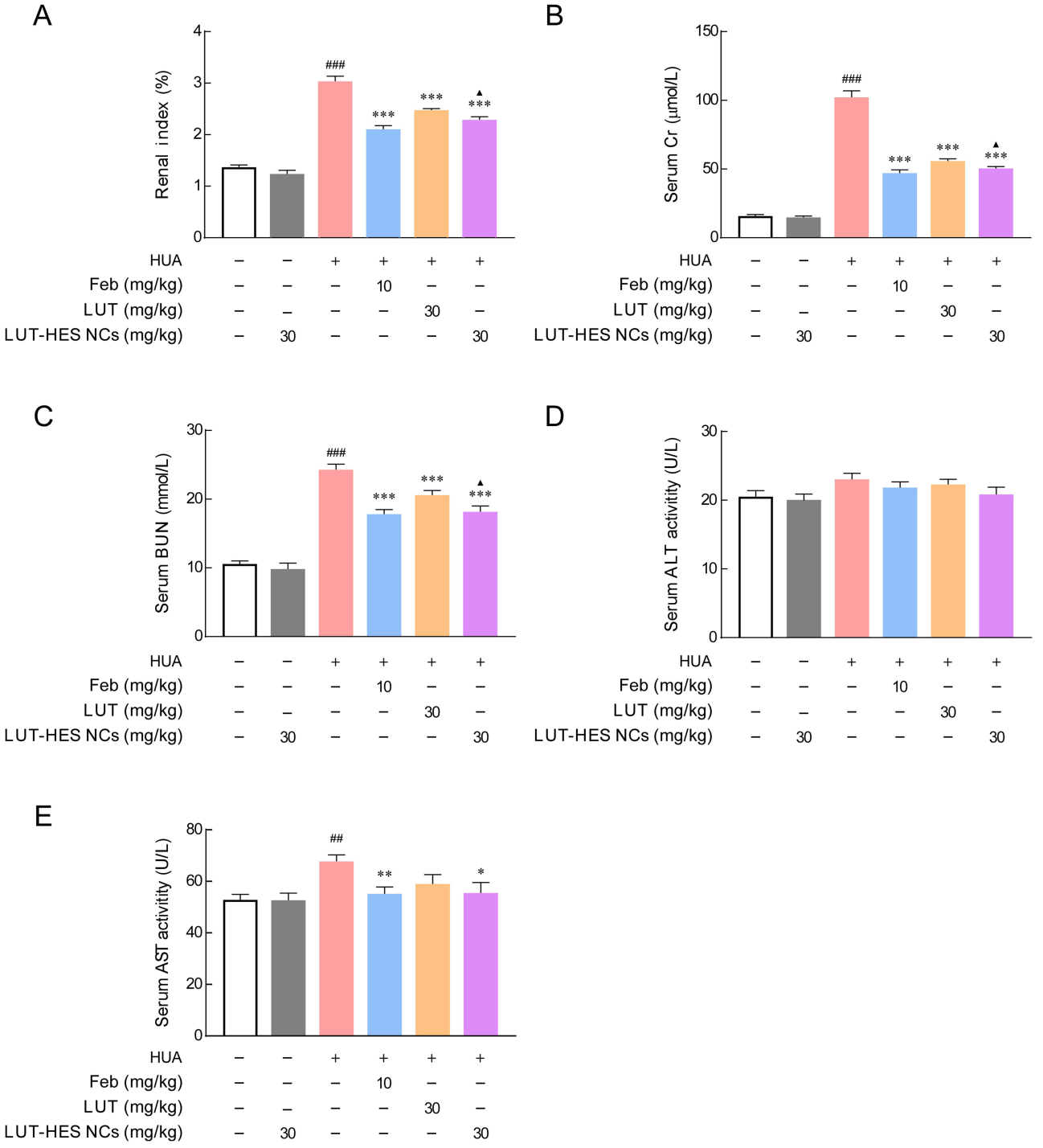


**Figure 10** The effect of LUT-HES NCs on the hepatic and renal function of HUA mice: (**A**) renal index; (**B**–**E**) serum Cr, BUN, ALT and AST levels.
**Notes**: Data are reported as mean ± SEM, n=8. ##*P*<0.01, ###*P*<0.001, versus the control group; **P*<0.05, ***P*<0.01, ****P*<0.001, versus the model group; ▲*P*<0.05, versus the LUT group.
**Abbreviations**: LUT, luteolin; HES, hydroxyethyl starch; NCs, nanocrystals; LUT-HES NCs, HES-stabilized LUT NCs; Feb, febuxostat; HUA, hyperuricemia; Cr, creatinine; BUN, blood urea nitrogen; ALT, alanine aminotransferase; AST, aspartate aminotransferase.

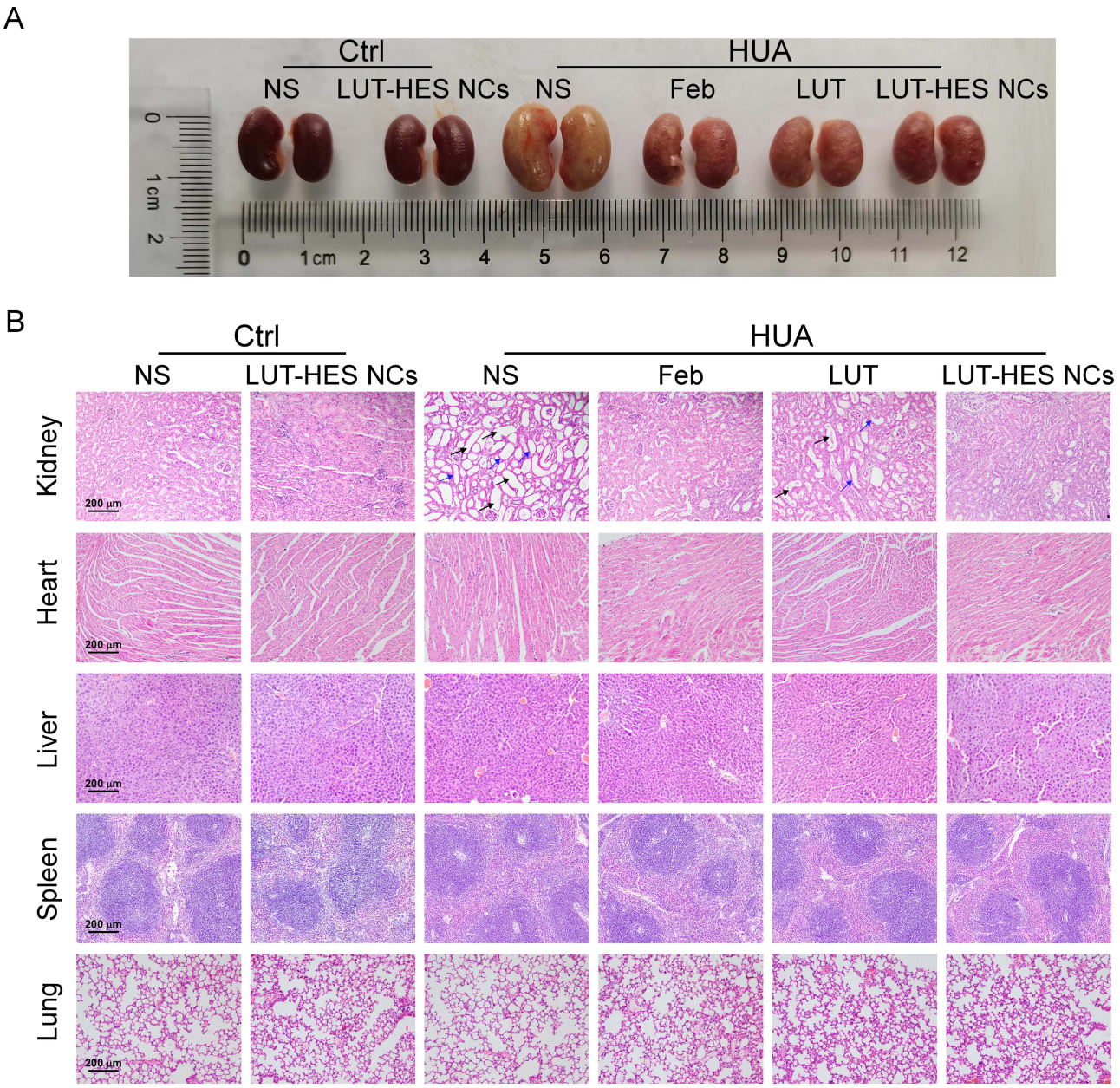


**Figure 11** Representative external photos of kidney (**A**) and representative histopathological images of organs (kidney, heart, liver, spleen and lung) (**B**) from mice with different treatment.

**Notes**: The black arrow indicates the renal tubular dilation. The blue arrow indicates the tubular epithelium atrophy.

**Abbreviations**: LUT, luteolin; HES, hydroxyethyl starch; NCs, nanocrystals; LUT-HES NCs, HES-stabilized LUT NCs; Feb, febuxostat; NS, normal saline; HUA, hyperuricemia; Crtl, control.

morphology (yellowish color), tubular dilation and tubular epithelium atrophy, accompanied by an elevated renal index and markedly increased BUN and Scr concentrations in comparison with the normal group. These results suggested that there was severe renal injury in hyperuricemic mice. After treatment with free LUT and LUT-HES NCs, the kidneys showed varying degrees of recovery in function (Figure 10A–C) and histological morphology (Figure 11). Kidneys in the LUT-HES NCs group were closer to those in the normal group than in the free LUT group, demonstrating that LUT-HES NCs had a better organ-protective effect on uric acid-induced renal damage than free LUT. In addition, the LUT-HES NCs did not cause damage to other tissues (Figures 10D, E and 11B), and exert on influence on biological indicators of normal mice (Figures 9–11). Collectively, these results demonstrated that LUT-HES NCs effectively improved the organ protection of LUT in hyperuricemic mice with great safety.

## Conclusion

The present work revealed the potential of HES as a prominent stabilizer for poorly soluble flavonoid nanocrystals. Uniform HES-stabilized LUT NCs, quercetin NCs, hesperidin NCs, and baicalin NCs were prepared. The LUT-HES NCs with the diameter of approximately 200 nm showed increased intestinal absorption and oral bioavailability, which significantly lowered serum uric acid levels and ameliorated hyperuricemia-induced kidney injury against HUA mice. The effect of LUT-HES NCs for gout management can be further explored in the follow-up study since luteolin is reported to exhibit strong anti-inflammatory activity. This study not only provides new insights for the clinical application of these compounds, but also offers an alternative or complementary strategy for the treatment of hyperuricemia.

## Data Sharing Statement

All datasets supporting this study are available from the corresponding author on reasonable request.

## Ethics Statement

All animal experiments were evaluated, approved, and supervised by the Ethics Committee on Animal Experiments of Hubei University of Medicine (approval number: SYXK2019–0031) and conformed to the guideline for the ethical review of laboratory animal welfare (People's Republic of China National Standard GB/T 35892–2018).

## Acknowledgment

Han Luo and Xiaofei Wang contributed equally to this work and are co-first authors. The authors would like to thank the Biomedical Research Institute of Hubei University of Medicine and Ceshigo for providing the laboratory accommodation. Furthermore, the authors would like to thank Meijuan Chen, Yuxuan Huang, Lili Yang and Yuzhi Sheng for their support in animal experiments.

## Funding

This study was funded by the Natural Science Foundation of Hubei Provincial Department of Education (Grant No. Q20222115, Grant No. D20192101), the Cultivating Project for Young Scholar at Hubei University of Medicine (Grant No. 2021QDJZR017), the Innovation and Entrepreneurship Training Program for College Students in Hubei Province (Grant No. S202210929011), and the Innovative Research Program for Graduates of Hubei University of Medicine (Grant No. YC2023067).

## Disclosure

The authors declare no conflicts of interest related to this study.

## References

1. Al-Khayri JM, Sahana GR, Nagella P, Joseph BV, Alessa FM, Al-Mssallem MQ. Flavonoids as potential anti-inflammatory molecules: a review. *Molecules*. 2022;27(9):2901. doi:10.3390/molecules27092901
2. Teng H, Zheng Y, Cao H, Huang Q, Xiao J, Chen L. Enhancement of bioavailability and bioactivity of diet-derived flavonoids by application of nanotechnology: a review. *Crit Rev Food Sci Nutr*. 2023;63(3):378–393. doi:10.1080/10408398.2021.1947772
3. Vazhappilly CG, Amararathna M, Cyril AC, et al. Current methodologies to refine bioavailability, delivery, and therapeutic efficacy of plant flavonoids in cancer treatment. *J Nutr Biochem*. 2021;94:108623. doi:10.1016/j.jnutbio.2021.108623
4. Shen N, Wang T, Gan Q, Liu S, Wang L, Jin B. Plant flavonoids: classification, distribution, biosynthesis, and antioxidant activity. *Food Chem*. 2022;383:132531. doi:10.1016/j.foodchem.2022.132531
5. Xiao J. Recent advances in dietary flavonoids for management of type 2 diabetes. *Curr Opin Food Sci*. 2022;4:1100806.
6. Adachi S, Oyama M, Kondo S, Yagasaki K. Comparative effects of quercetin, luteolin, apigenin and their related polyphenols on uric acid production in cultured hepatocytes and suppression of purine bodies-induced hyperuricemia by rutin in mice. *Cytotechnology*. 2021;73(3):343–351. doi:10.1007/s10616-021-00452-9
7. Siddiqui SS, Rahman S, Rupasinghe HV, Vazhappilly CG. Dietary flavonoids in p53—mediated immune dysfunctions linking to cancer prevention. *Biomedicines*. 2020;8(8):286. doi:10.3390/biomedicines8080286
8. Vazhappilly CG, Ansari SA, Al-Jaleeli R, et al. Role of flavonoids in thrombotic, cardiovascular, and inflammatory diseases. *Inflammopharmacology*. 2019;27(5):863–869. doi:10.1007/s10787-019-00612-6
9. Xu Q, Zhang W, Xu H, Zhang Q. Fabrication of luteolin loaded zein-caseinate nanoparticles and its bioavailability enhancement in rats. *J Pharm Sci*. 2023;112(13):3056–3066. doi:10.1016/j.xphs.2023.06.010

10. Zhao J, Yang J, Xie Y. Improvement strategies for the oral bioavailability of poorly water-soluble flavonoids: an overview. *Int J Pharm*. 2019;570:118642. doi:10.1016/j.ijpharm.2019.118642
11. Xiang D, Wang C, Wang W, et al. Gastrointestinal stability of dihydromyricetin, myricetin, and myricitrin: an in vitro investigation. *Int J Food Sci Nutr*. 2017;68(6):704–711. doi:10.1080/09637486.2016.1276518
12. Gujar K, Wairkar S. Nanocrystal technology for improving therapeutic efficacy of flavonoids. *Phytomedicine*. 2020;71:153240. doi:10.1016/j.phymed.2020.153240
13. Liu J, Sun Y, Cheng M, et al. Improving oral bioavailability of luteolin nanocrystals by surface modification of sodium dodecyl sulfate. *AAPS PharmSciTech*. 2021;22(3):133. doi:10.1208/s12249-021-02012-y
14. Liu J, Tu L, Cheng M, Feng J, Jin Y. Mechanisms for oral absorption enhancement of drugs by nanocrystals. *J Drug Deliv Sci Technol*. 2020;56:101607. doi:10.1016/j.jddst.2020.101607
15. Wang Y, Tan X, Fan X, et al. Current strategies for oral delivery of BCS IV drug nanocrystals: challenges, solutions and future trends. *Expert Opin Drug Deliv*. 2021;18(9):1211–1228. doi:10.1080/17425247.2021.1903428
16. Ghadi R, Dand N. BCS class IV drugs: highly notorious candidates for formulation development. *J Control Release*. 2017;248:71–95. doi:10.1016/j.jconrel.2017.01.014
17. Pardhi E, Vasave R, Srivastava V, Yadav R, Mehra NK. Nanocrystal technologies in biomedical science: from the bench to the clinic. *Drug Discov Today*. 2022;29(3):103913. doi:10.1016/j.drudis.2024.103913
18. Long J, Song J, Zhang X, et al. Tea saponins as natural stabilizers for the production of hesperidin nanosuspensions. *Int J of Pharm*. 2020;583:119406. doi:10.1016/j.ijpharm.2020.119406
19. Tu L, Cheng M, Sun Y, et al. Fabrication of ultra-small nanocrystals by formation of hydrogen bonds: in vitro and in vivo evaluation. *Int J Pharm*. 2020;573:118730. doi:10.1016/j.ijpharm.2019.118730
20. Suo Z, Sun Q, Peng X, et al. Lentinan as a natural stabilizer with bioactivities for preparation of drug-drug nanosuspensions. *Int J Biol Macromol*. 2021;184:101–108. doi:10.1016/j.ijbiomac.2021.06.056
21. Luo Y, Liu Y, Chen Y, et al. Study on redispersibility of drug nanocrystals particles during storage: novel understanding based on water adsorption and glass transition of amorphous matrix formers. *Int J Pharm*. 2020;575:118945. doi:10.1016/j.ijpharm.2019.118945
22. Wang H, Hu H, Yang H, Li Z. Hydroxyethyl starch based smart nanomedicine. *RSC Adv*. 2021;11(6):3226–3240. doi:10.1039/D0RA09663F
23. Xiao C, Li J, Wang X, et al. Hydroxyethyl starch stabilized copper-diethyldithiocarbamate nanocrystals for cancer therapy. *J Control Release*. 2023;356:288–305. doi:10.1016/j.jconrel.2023.02.043
24. Li J, Yang Y, Lu L, Ma Q, Zhang J. Preparation, characterization and systemic application of self-assembled Hydroxyethyl starch nanoparticles-loaded flavonoid Morin for hyperuricemia therapy. *Int J Nanomedicine*. 2018;13:2129–2141. doi:10.2147/IJN.S158585
25. Zarbock AMD, Buhre WMD. Hydroxyethyl starch in the perioperative period: friend, foe, or still an unsolved issue? *Anesth Analg*. 2022;134(4):683–685. doi:10.1213/ANE.0000000000005903
26. Xiong Y, Wang Z, Wang Q, et al. Tumor-specific activatable biopolymer nanoparticles stabilized by hydroxyethyl starch prodrug for self-amplified cooperative cancer therapy. *Theranostics*. 2022;12(2):944–962. doi:10.7150/thno.67572
27. Stolzing A, Naaldijk Y, Fedorova V, Sethe S. Hydroxyethylstarch in cryopreservation - mechanisms, benefits and problems. *Transfus Apher Sci*. 2012;46(2):137–147. doi:10.1016/j.transci.2012.01.007
28. Lin Y, Liu P, Liang W, et al. Luteolin-4′-O-glucoside and its aglycone, two major flavones of Gnaphalium affine D. Don, resist hyperuricemia and acute gouty arthritis activity in animal models. *Phytomedicine*. 2018;41:54–61. doi:10.1016/j.phymed.2018.02.002
29. Yue P, Li Y, Wan J, et al. Process optimization and evaluation of novel baicalin solid nanocrystals. *Int J Nanomedicine*. 2013;8:2961–2973. doi:10.2147/IJN.S44924
30. Weng W, Wang Q, Wei C, et al. Preparation, characterization, pharmacokinetics and anti-hyperuricemia activity studies of myricitrin-loaded proliposomes. *Int J Pharm*. 2019;572:118735. doi:10.1016/j.ijpharm.2019.118735
31. Khan BA, Rashid F, Khan MK, Alqahtani SS, Sultan MH, Almoshari Y. Fabrication of capsaicin loaded nanocrystals: physical characterizations and in vivo evaluation. *Pharmaceutics*. 2021;13(841):1–14. doi:10.3390/pharmaceutics13060841
32. Zhang T, Li X, Xu J, Shao J, Ding M, Shi S. Preparation, Characterization, and evaluation of breviscapine nanosuspension and its freeze-dried powder. *Pharmaceutics*. 2022;14(923):1–19 doi:10.3390/pharmaceutics14050923.
33. Yang X, Sheng J, Chen J, et al. The effect of Longan Arillus extract on enhancing oral absorption of bioactive peptides derived from defatted walnut meal hydrolysates. *J Funct Foods*. 2019;57:309–316. doi:10.1016/j.jff.2019.04.018
34. Hernández GA, López BA, García MN, et al. Nanosuspensions as carriers of active ingredients: chemical composition, development methods, and their biological activities. *Food Res Int*. 2023;174:113583. doi:10.1016/j.foodres.2023.113583
35. Ao H, Li Y, Li H, et al. Preparation of hydroxy genkwanin nanosuspensions and their enhanced antitumor efficacy against breast cancer. *Drug Deliv*. 2020;27(1):816–824. doi:10.1080/10717544.2020.1770372
36. Zhou Y, Fang Q, Niu B, et al. Comparative studies on amphotericin B nanosuspensions prepared by a high pressure homogenization method and an antisolvent precipitation method. *Colloids Surf B Biointerfaces*. 2018;172:372–379. doi:10.1016/j.colsurfb.2018.08.016
37. Liu K, Zha X, Li Q, Pan L, Luo J. Hydrophobic interaction and hydrogen bonding driving the self-assembling of quinoa protein and flavonoids. *Food Hydrocolloids*. 2021;118:106807. doi:10.1016/j.foodhyd.2021.106807
38. Li Q, Chen F, Liu Y, et al. A novel albumin wrapped nanosuspension of meloxicam to improve inflammation-targeting effects. *Int J Nanomedicine*. 2018;13:4711–4725. doi:10.2147/IJN.S160714
39. Müller RH, Peters K, Xie L, Liu K, Zhang X, Li X. Preparation and characterization of quercetin nanosuspensions using gypenosides as novel stabilizers. *J Drug Deliv Sci Technol*. 2022;67:102962. doi:10.1016/j.jddst.2021.102962
40. Panse N, Gerk PK. The Caco-2 Model: modifications and enhancements to improve efficiency and predictive performance. *Int J Pharm*. 2022;25:122004. doi:10.1016/j.ijpharm.2022.122004
41. Deng F, Zhang H, Wang X, et al. Transmembrane pathways and mechanisms of rod-like paclitaxel nanocrystals through MDCK polarized monolayer. *ACS Appl Mater Interfaces*. 2017;9(7):5803–5816. doi:10.1021/acsami.6b15151
42. Patel S, Kim J, Herrera M, Mukherjee A, Kabanov AV, Sahay G. Brief update on endocytosis of nanomedicines. *Adv Drug Deliv Rev*. 2019;144:90–111. doi:10.1016/j.addr.2019.08.004

43. Yang M, Lu X, Xu J, et al. Cellular uptake, transport mechanism and anti-inflammatory effect of cyanidin-3-glucoside nanoliposomes in Caco-2/RAW 264.7 co-culture model. *Front Nutr*. 2022;9:995391. doi:10.3389/fnut.2022.995391
44. Zhang Z, Tao Q, Qin Z, et al. Uptake and transport of naringenin and its antioxidant effects in human intestinal epithelial Caco-2 cells. *Front Nutr*. 2022;24(9):894117. doi:10.3389/fnut.2022.894117
45. Kojima S, Uchiyama K, Yokota N, et al. Optimal uric acid levels by febuxostat treatment and cerebral, cardiorenovascular risks: post hoc analysis of a randomized controlled trial. *Rheumatology*. 2022;61(6):2346–2359. doi:10.1093/rheumatology/keab739
46. Hu Q, Lan H, Tian Y, et al. Biofunctional coacervate-based artificial protocells with membrane-like and cytoplasm-like structures for the treatment of persistent hyperuricemia. *J Contr Release*. 2024;365:176–192. doi:10.1016/j.jconrel.2023.11.030
47. Wei C, Wang Q, Weng W, et al. Enhanced oral bioavailability and anti-hyperuricemic activity of liquiritin via a self-nanoemulsifying drug delivery system. *J Sci Food Agric*. 2022;102(5):2032–2040. doi:10.1002/jsfa.11542

**International Journal of Nanomedicine** Dovepress

## Publish your work in this journal

The International Journal of Nanomedicine is an international, peer-reviewed journal focusing on the application of nanotechnology in diagnostics, therapeutics, and drug delivery systems throughout the biomedical field. This journal is indexed on PubMed Central, MedLine, CAS, SciSearch®, Current Contents®/Clinical Medicine, Journal Citation Reports/Science Edition, EMBase, Scopus and the Elsevier Bibliographic databases. The manuscript management system is completely online and includes a very quick and fair peer-review system, which is all easy to use. Visit http://www.dovepress.com/testimonials.php to read real quotes from published authors.

**Submit your manuscript here:** https://www.dovepress.com/international-journal-of-nanomedicine-journal